J|A|C|S ARTICLES

Published on Web 12/17/2009

Uniform Mesoporous Dye-Doped Silica Nanoparticles Decorated with Multiple Magnetite Nanocrystals for Simultaneous Enhanced Magnetic Resonance Imaging, Fluorescence Imaging, and Drug Delivery

Ji Eun Lee,[†] Nohyun Lee,[†] Hyoungsu Kim,[‡] Jaeyun Kim,[†] Seung Hong Choi,[‡] Jeong Hyun Kim,[†] Taeho Kim,[†] In Chan Song,[‡] Seung Pyo Park,[†] Woo Kyung Moon,[‡] and Taeghwan Hyeon*[,†]

National Creative Research Initiative Center for Oxide Nanocrystalline Materials, and School of Chemical and Biological Engineering, Seoul National University, Seoul 151-744, Korea, and Diagnostic Radiology, Seoul National University Hospital, and Institute of Radiation Medicine, Medical Research Center, Seoul National University, 28, Yeongeon-dong, Jongno-gu, Seoul 110-744, Korea

Received July 13, 2009; E-mail: thyeon@snu.ac.kr

Abstract: Highly versatile nanocomposite nanoparticles were synthesized by decorating the surface of mesoporous dye-doped silica nanoparticles with multiple magnetite nanocrystals. The superparamagnetic property of the magnetite nanocrystals enabled the nanoparticles to be used as a contrast agent in magnetic resonance (MR) imaging, and the dye molecule in the silica framework imparted optical imaging modality. Integrating a multitude of magnetite nanocrystals on the silica surface resulted in remarkable enhancement of MR signal due to the synergistic magnetism. An anticancer drug, doxorubicin (DOX), could be loaded in the pores and induced efficient cell death. In vivo passive targeting and accumulation of the nanoparticles at the tumor sites was confirmed by both T2 MR and fluorescence imaging. Furthermore, apoptotic morphology was clearly detected in tumor tissues of mice treated with DOX loaded nanocomposite nanoparticles, demonstrating that DOX was successfully delivered to the tumor sites and its anticancer activity was retained.

Introduction

Many types of nanostructured materials have been investigated for their potential applications in biomedical imaging, diagnostics, and therapy.[1] In particular, colloidal nanoparticles have been extensively investigated as probes in biomedical imaging due to their unique size-dependent electronic, optical, and magnetic properties.[2] For example, magnetic nanoparticles have been used as T2 magnetic resonance imaging (MRI) contrast agents.[3] Semiconductor nanoparticles, also known as quantum dots, have been used as fluorescent probes in cell labeling, tracking, and imaging.[4] Au nanoparticles have been used in sensing cDNA.[5] On the other hand, mesoporous silica materials with large pore volumes[6] have been investigated for their potential use as drug delivery vehicles.[7,8] Combining different nanostructured materials will enable the development of multifunctional nanomedical platforms for multimodal imaging or simultaneous diagnosis and therapy.[9] Recently, Prasad et al. reported the fabrication of multifunctional nanoprobes for

[†] National Creative Research Initiative Center for Oxide Nanocrystalline Materials, and School of Chemical and Biological Engineering.

[‡] Seoul National University Hospital, and Institute of Radiation Medicine, Medical Research Center.

(1) (a) Klabunde, K. J., Ed. *Nanoscale Materials in Chemistry*; Wiley-Interscience: New York, 2001. (b) Ozin, G. A.; Arsenault, A.; Cademartiri, L. *Nanochemistry: A Chemical Approach to Nanomaterials Nanochemistry*, 2nd ed.; RSC Publishing: Cambridge, UK, 2008. (c) Schmid, G. *Nanoparticles: From Theory to Application*; Wiley-VCH: Weinheim, 2004.

(2) (a) Alivisatos, A. P. *Nat. Biotechnol.* **2004**, *22*, 47. (b) Rosi, N. L.; Mirkin, C. A. *Chem. Rev.* **2005**, *105*, 1547. (c) Niemeyer, C. M.; Mirkin, C. A. *Nanobiotechnology: Concepts, Applications and Perspectives*; Wiley-VCH: Weinheim, 2004. (d) Michalet, X.; Pinaud, F. F.; Bentolila, L. A.; Tsay, J. M.; Doose, S.; Li, J. J.; Sundaresan, G.; Wu, A. M.; Gambhir, S. S.; Weiss, S. *Science* **2005**, *307*, 538.

(3) (a) Weissleder, R.; Moore, A.; Mahmood, U.; Bhorade, R.; Benveniste, H.; Chiocca, E. A.; Basilion, J. P. *Nat. Med.* **2000**, *6*, 351. (b) Zhao, M.; Beauregard, D. A.; Loizou, L.; Davletov, B.; Brindle, K. M. *Nat. Med.* **2001**, *1*, 1241. (c) Bulte, J. W. M.; Douglas, T.; Witwer, B.; Zhang, S.-C.; Strable, E.; Lewis, B. K.; Zywicke, H.; Miller, B.; van Gelderen, P.; Moskowitz, B. M.; Duncan, I. D.; Frank, J. A. *Nat. Biotechnol.* **2001**, *19*, 1141. (d) de Vries, I. J. M.; Lesterhuis, W. J.; Barentsz, J. O.; Verdijk, P.; van Krieken, J. H.; Boerman, O. C.; Oyen, W. J. G.; Bonenkamp, J. J.; Boezeman, J. B.; Adema, G. J.; Bulte, J. W. M.; Scheenen, T. W. J.; Punt, C. J. A.; Heerschap, A.; Figdor, C. G. *Nat. Biotechnol.* **2005**, *23*, 1407. (e) Medarova, Z.; Pham, W.; Farrar, C.; Petkova, V.; Moore, A. *Nat. Med.* **2007**, *13*, 372. (f) Bulte, J. W. M.; Kraitchman, D. L. *NMR Biomed.* **2004**, *17*, 484. (g) Na, H. B.; Song, I. C.; Hyeon, T. *Adv. Mater.* **2009**, *21*, 2133. (h) Jun, Y.-W.; Seo, J.-W.; Cheon, J. *Acc. Chem. Res.* **2008**, *41*, 179.

(4) (a) Gao, X.; Cui, Y.; Levenson, R. M.; Chung, L. W. K.; Nie, S. *Nat. Biotechnol.* **2004**, *22*, 969. (b) Medintz, I. L.; Uyeda, H. T.; Goldman, E. R.; Mattoussi, H. *Nat. Mater.* **2005**, *4*, 435. (c) Dubertret, B.; Skourides, P.; Norris, D. J.; Noireaux, V.; Brivanlou, A. H.; Libchaber, A. *Science* **2002**, *298*, 1759. (d) Larson, D. R.; Zipfel, W. R.; Williams, R. M.; Clark, S. W.; Bruchez, M. P.; Wise, F. W.; Webb, W. W. *Science* **2003**, *300*, 1434. (e) Klostranec, J. M.; Chan, W. C. W. *Adv. Mater.* **2006**, *18*, 1953. (f) Kim, S.; Lim, Y. T.; Soltesz, E. G.; De Grand, A. M.; Lee, J.; Nakayama, A.; Parker, J. A.; Mihaljevic, T.; Laurence, R. G.; Dor, D. M.; Cohn, L. H.; Bawendi, M. G.; Frangioni, J. V. *Nat. Biotechnol.* **2004**, *22*, 93. (g) Selvan, S. T.; Patra, P. K.; Ang, C. Y.; Ying, J. Y. *Angew. Chem., Int. Ed.* **2007**, *46*, 2448.

10.1021/ja905793q

imaging live cancer cells by coencapsulation of quantum dots and magnetite nanoparticles within organically modified silica. They also fabricated a biocompatible ferrofluid containing dye-functionalized magnetite nanoparticles and demonstrated optical tracking of basic processes at the cellular level combined with magnetophoretic manipulation.[10] Herein, we report the fabrication of uniform mesoporous dye-doped silica nanoparticles immobilized with multiple magnetite nanocrystals on the surface (designated as Fe_3O_4-MSN) as well as their applications to simultaneous MRI, fluorescence imaging, and as a drug delivery vehicle. The integration of numerous magnetite nanocrystals on the silica surface resulted in synergistic magnetism that enhanced the MR signal.[11] Small dye molecules incorporated in the silica framework imparted optical imaging modality.[12] In addition, anticancer drug was able to be loaded into the pores of mesoporous silica nanoparticles for drug delivery. We also demonstrated in vivo passive targeting of the nanocomposite particles to tumors.

Experimental Section

Synthesis of Mesoporous Silica Nanoparticle (MSN). Dye-doped MSN was synthesized by modifying a previously reported method.[8] Rhodamine B isothiocyanate (RITC, Aldrich) (5 mg) or fluorescein isothiocyanate (FITC, Aldrich) (4 mg) was reacted with 44 μL of 3-aminopropyltriethoxysilane (APS, Sigma, 98%) (molar ratio of dye:APS = 1:10) in 1 mL of ethanol overnight in the dark. NaOH (0.35 mL, 2 M) was added to 50 mL of cetyltrimethylammonium bromide (CTAB, Acros, 99+%) solution (0.1 g in 50 mL of water). The mixture was heated to 70 °C, followed by the addition of 0.5 mL of tetraethylorthosilicate (TEOS, Acros, 98%) and 50 μL of APS-modified dye solution. After 1 min, 0.5 mL of ethyl acetate (EtOAc, Samchun, 99.5%) was added, and the resulting mixture was stirred at 70 °C for 30 s and then aged for 2 h. The precipitate was collected by centrifugation and washed with water and ethanol four times. Finally, the pore-generating template, CTAB, was removed by refluxing in acidic ethanol solution. A JEM-2010 transmission electron microscope (JEOL) was used for the transmission electron microscopy (TEM) analysis. The average size of MSN was estimated by measuring the sizes of over 200 particles.

Surface Modification of MSN. The surface of MSN was functionalized with amine groups by treatment with APS. MSN (0.1 mg) was dispersed in 10 mL of ethanol. The solution was refluxed for 3 h, followed by the addition of 40 μL of APS. After centrifugation and washing with ethanol, amine-functionalized MSN was redispersed in 5 mL of ethanol.

Ligand Exchange of Fe_3O_4 Nanocrystals. Monodisperse Fe_3O_4 nanocrystals capped with oleic acid were synthesized in organic solution via previously reported procedures.[13] 2-Bromo-2-methylpropionic acid (BMPA, Aldrich, 98%) (0.5 g) and citric acid (Samchun) (0.05 g) were dissolved in a mixture of chloroform and DMF (50/50 v/v, 15 mL).[14] The synthesized nanocrystals (15 mg) were dispersed in the BMPA solution and stirred overnight at 30 °C. Finally, the ligand-exchanged nanocrystals were retrieved by centrifugation and redispersed in 5 mL of ethanol.

Synthesis of Fe_3O_4-MSN and Surface Modification with PEG. The amine-functionalized MSN dispersion (1 mL) was reacted with 5 mL of the ligand-exchanged Fe_3O_4 nanocrystals dispersion. The Fe_3O_4-MSN was retrieved by centrifugation and washed with ethanol to remove excess Fe_3O_4 nanocrystals. The resulting Fe_3O_4-MSN was mixed with 25 mg of methoxy poly(ethylene glycol) succinimidyl glutarate (mPEG-SG, MW 5000, Sunbio) dissolved in 5 mL of ethanol. The mixture was stirred overnight at 30 °C to induce covalent bonding between residual amine groups on the surface of MSN and succinimidyl groups of the PEG. After removal of unreacted mPEG-SG by centrifugation, 25 mg of methoxy

(5) (a) Elghanian, R.; Storhoff, J. J.; Mucic, R. C.; Letsinger, R. L.; Mirkin, C. A. *Science* **1997**, *277*, 1078. (b) Jin, R.; Wu, G.; Li, Z.; Mirkin, C. A.; Schatz, G. C. *J. Am. Chem. Soc.* **2003**, *125*, 1643. (c) Taton, T. A.; Mirkin, C. A.; Letsinger, R. L. *Science* **2000**, *289*, 1757. (d) Nam, J. M.; Thaxton, C. S.; Mirkin, C. A. *Science* **2003**, *301*, 1884.

(6) (a) Ying, J. Y.; Mehnert, C. P.; Wong, M. S. *Angew. Chem., Int. Ed.* **1999**, *38*, 56. (b) Davis, M. E. *Nature* **2002**, *417*, 813. (c) Wan, Y.; Zhao, D. *Chem. Rev.* **2007**, *107*, 2821.

(7) Vallet-Regí, M.; Balas, F.; Arcos, D. *Angew. Chem., Int. Ed.* **2007**, *46*, 7548.

(8) (a) Slowing, I. I.; Trewyn, B. G.; Giri, S.; Lin, V. S.-Y. *Adv. Funct. Mater.* **2007**, *17*, 1225. (b) Torney, F.; Trewyn, B. G.; Lin, V. S.-Y.; Wang, K. *Nat. Nanotechnol.* **2007**, *2*, 295. (c) Hsiao, J.-K.; Tsai, C.-P.; Chung, T.-H.; Hung, Y.; Yao, M.; Liu, H.-M.; Mou, C.-Y.; Yang, C.-S.; Chen, Y.-C.; Huang, D.-M. *Small* **2008**, *4*, 1445. (d) Vivero-Escoto, J. L.; Slowing, I. I.; Wu, C.-W.; Lin, V. S.-Y. *J. Am. Chem. Soc.* **2009**, *131*, 3462. (e) Slowing, I. I.; Vivero-Escoto, J. L.; Wu, C.-W.; Lin, V. S.-Y. *Adv. Drug Delivery Rev.* **2008**, *60*, 1278. (f) Trewyn, B. G.; Slowing, I. I.; Giri, S.; Chen, H.-T.; Lin, V. S.-Y. *Acc. Chem. Res.* **2007**, *40*, 846. (g) Lai, C.-Y.; Trewyn, B. G.; Jeftinija, D. M.; Jeftinija, K.; Xu, S.; Jeftinija, S.; Lin, V. S.-Y. *J. Am. Chem. Soc.* **2003**, *125*, 4451. (h) Giri, S.; Trewyn, B. G.; Stellmaker, M. P.; Lin, V. S.-Y. *Angew. Chem., Int. Ed.* **2005**, *44*, 5038. (i) Lin, V. S.-Y.; Lai, C. Y.; Huang, J. G.; Song, S. A.; Xu, S. *J. Am. Chem. Soc.* **2001**, *123*, 11510. (j) Slowing, I. I.; Trewyn, B. G.; Lin, V. S.-Y. *J. Am. Chem. Soc.* **2007**, *129*, 8845. (k) Taylor, K. M. L.; Kim, J. S.; Rieter, W. J.; An, H.; Lin, W.; Lin, W. *J. Am. Chem. Soc.* **2008**, *130*, 2154. (l) Trewyn, B. G.; Giri, S.; Slowing, I. I.; Lin, V. S.-Y. *Chem. Commun.* **2007**, 323. (m) Rosenholm, J. M.; Meinander, A.; Peuhu, E.; Niemi, R.; Eriksson, J. E.; Sahlgren, C.; Lindén, M. *ACS Nano* **2009**, *3*, 197.

(9) (a) Kim, J.; Piao, Y.; Hyeon, T. *Chem. Soc. Rev.* **2009**, *38*, 372. (b) Nasongkla, N.; Bey, E.; Ren, J.; Ai, H.; Khemtong, C.; Guthi, J. S.; Chin, S.-F.; Sherry, A. D.; Boothman, D. A.; Gao, J. *Nano Lett.* **2006**, *6*, 2427. (c) Kim, J.; Park, S.; Lee, J. E.; Jin, S. M.; Lee, J. H.; Lee, I. S.; Yang, I.; Kim, J.-S.; Kim, S. K.; Cho, M.-H.; Hyeon, T. *Angew. Chem., Int. Ed.* **2006**, *45*, 7754. (d) Lee, J.-H.; Jun, Y.-w.; Yeon, S.-I.; Shin, J.-S.; Cheon, J. *Angew. Chem., Int. Ed.* **2006**, *45*, 8160. (e) Rieter, W. J.; Kim, J. S.; Taylor, K. M. L.; An, H.; Lin, W.; Tarrant, T.; Lin, W. *Angew. Chem., Int. Ed.* **2007**, *46*, 3680. (f) Xu, C.; Xie, J.; Ho, D.; Wang, C.; Kohler, N.; Walsh, E. G.; Morgan, J. R.; Chin, Y. E.; Sun, S. *Angew. Chem., Int. Ed.* **2008**, *47*, 173. (g) Lin, Y.-S.; Wu, S.-H.; Hung, Y.; Chou, Y.-H.; Chang, C.; Lin, M.-L.; Tsai, C.-P.; Mou, C.-Y. *Chem. Mater.* **2006**, *18*, 5170. (h) Kim, J.; Lee, J. E.; Lee, S. H.; Yu, J. H.; Lee, J. H.; Park, T. G.; Hyeon, T. *Adv. Mater.* **2008**, *20*, 478. (i) Kim, J.; Kim, H. S.; Lee, N.; Kim, T.; Kim, H.; Yu, T.; Song, I. C.; Moon, W. K.; Hyeon, T. *Angew. Chem., Int. Ed.* **2008**, *47*, 8438. (j) Liong, M.; Lu, J.; Kovochich, M.; Xia, T.; Ruehm, S. G.; Nel, A. E.; Tamanoi, F.; Zink, J. I. *ACS Nano* **2008**, *2*, 889. (k) van Schooneveld, M. M.; Vucic, E.; Koole, R.; Zhou, Y.; Stocks, J.; Cormode, D. P.; Tang, C. Y.; Gordon, R. E.; Nicolay, K.; Meijerink, A.; Fayad, Z. A.; Mulder, W. J. M. *Nano Lett.* **2008**, *8*, 2517. (l) Kim, J. S.; Rieter, W. J.; Taylor, K. M. L.; An, H.; Lin, W.; Lin, W. *J. Am. Chem. Soc.* **2007**, *129*, 8962. (m) Bridot, J.-L.; Faure, A.-C.; Laurent, S.; Rivière, C.; Billotey, C.; Hiba, B.; Janier, M.; Josserand, V.; Coll, J.-L.; Elst, L. V.; Muller, R.; Roux, S.; Perriat, P.; Tillement, O. *J. Am. Chem. Soc.* **2007**, *129*, 5076. (n) Wang, Y.; Caruso, F. *Chem. Mater.* **2005**, *17*, 953.

(10) (a) Law, W.-C.; Yong, K.-T.; Roy, I.; Xu, G.; Ding, H.; Bergey, E. J.; Zeng, H.; Prasad, P. N. *J. Phys. Chem. C* **2008**, *112*, 7972. (b) Sahoo, Y.; Goodarzi, A.; Swihart, M. T.; Ohulchanskyy, T. Y.; Kaur, N.; Furlani, E. P.; Prasad, P. N. *J. Phys. Chem. B* **2005**, *109*, 3879. (c) Cinteza, L. O.; Ohulchanskyy, T. Y.; Sahoo, Y.; Bergey, E. J.; Pandey, R. K.; Prasad, P. N. *Mol. Pharmacol.* **2006**, *2*, 415.

(11) (a) Josephson, L.; Perez, J. M.; Weissleder, R. *Angew. Chem., Int. Ed.* **2001**, *40*, 3204. (b) Perez, J. M.; Josephson, L.; O'Loughlin, T.; Höemann, D.; Weissleder, R. *Nat. Biotechnol.* **2002**, *20*, 816. (c) Berret, J.-F.; Schonbeck, N.; Gazeau, F.; El Kharrat, D.; Sandre, O.; Vacher, A.; Airiau, M. *J. Am. Chem. Soc.* **2006**, *128*, 1755. (d) Atanasijevic, T.; Shusteff, M.; Fam, P.; Jasanoff, A. *Proc. Natl. Acad. Sci. U.S.A.* **2006**, *103*, 14707.

(12) (a) Ow, H.; Larson, D. R.; Srivastava, M.; Baird, B. A.; Webb, W. W.; Wiesner, U. *Nano Lett.* **2005**, *5*, 113. (b) Burns, A.; Ow, H.; Wiesner, U. *Chem. Soc. Rev.* **2006**, *35*, 1028. (c) Burns, A. A.; Vider, J.; Ow, H.; Herz, E.; Penate-Medina, O.; Baumgart, M.; Larson, S. M.; Wiesner, U.; Bradbury, M. *Nano Lett.* **2009**, *9*, 442.

(13) Park, J.; An, K.; Hwang, Y.; Park, J.-G.; Noh, H.-J.; Kim, J.-Y.; Park, J.-H.; Hwang, N.-M.; Hyeon, T. *Nat. Mater.* **2004**, *3*, 891.

(14) (a) Wang, Y.; Teng, X.; Wang, J.-S.; Yang, H. *Nano Lett.* **2003**, *3*, 789. (b) Lattuada, M.; Hatton, T. A. *Langmuir* **2007**, *23*, 2158.

Scheme 1. Schematic Illustration of the Synthetic Procedure for Fe_3O_4-MSN

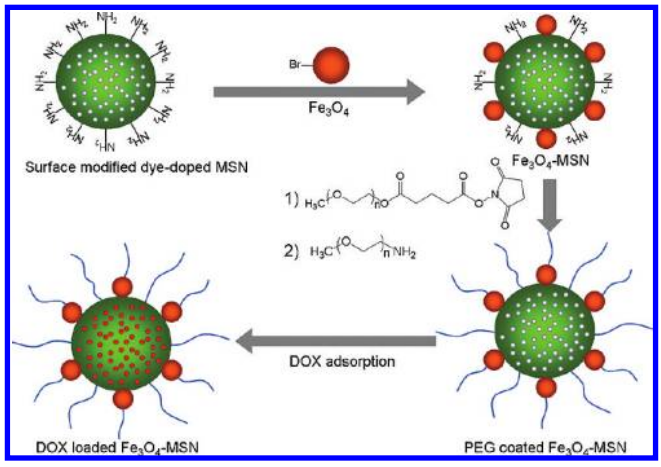

poly(ethylene glycol) amine (mPEG-AM, MW 5000, Sunbio) was subjected to the same procedure. The resulting PEG-stabilized Fe_3O_4-MSN was dispersed in water. Hydrodynamic diameter was measured by a dynamic light scattering (DLS) particle size analyzer (ELS-Z2, Otsuka).

Results and Discussion

Synthesis and Characterization of Fe_3O_4-MSN. The procedure for the fabrication of Fe_3O_4-MSN is illustrated in Scheme 1. To assemble Fe_3O_4 nanocrystals on the mesoporous dye-doped silica nanoparticles, the surface was functionalized with amine groups by treating with 3-aminopropyltriethoxysilane (APS). Oleic acid stabilized Fe_3O_4 nanocrystals, synthesized in an organic media,[13] were reacted with 2-bromo-2-methylpropionic acid (BMPA),[14] and the resulting Fe_3O_4 nanocrystals were assembled on the surfaces of MSN by direct nucleophilic substitution reaction between the terminal bromine groups of BMPA and the amine groups of the silica nanoparticles.[15] Polyethylene glycol (PEG), which is known to prevent nonspecific protein adsorption,[16] was used to make the nanocomposite nanoparticles biocompatible and well dispersible in aqueous media. After the Fe_3O_4 nanocrystals were immobilized on MSN, residual amine groups of the silica surface and bromine groups of the Fe_3O_4 nanocrystals were reacted with succinimidyl- and amine-modified PEG, respectively.

Figure 1a−c shows TEM images of the synthesized Fe_3O_4-MSN. The dye-doped MSN were discrete and uniform with an average diameter of 70 ± 6 nm, and well-ordered mesopores were also clearly observed (Figure 1a). Following immobilization of the 8.5 nm Fe_3O_4 nanocrystals, no aggregates were observed in the TEM images (Figure 1b,c). To impart fluorescence imaging capability, APS was covalently bonded to FITC or RITC, followed by co-condensation of the resulting APS-modified dye with TEOS during the MSN synthesis step. The dye-doped composite nanoparticles displayed typical emission peaks of fluorescein and rhodamine B at 520 and 576 nm, respectively (Figure 1d). The PEG-stabilized Fe_3O_4-MSN showed excellent colloidal stability in water. The dynamic light scattering (DLS) data (Figure S1 in the Supporting Information) showed PEG-stabilized Fe_3O_4-MSN had narrow size distribution with an overall hydrodynamic diameter of 93 nm in water. This demonstrated that the Fe_3O_4-MSN are stable in water and do not form aggregates. Surprisingly, even in culture media containing 10% fetal bovine serum, Fe_3O_4-MSN retain their narrow size distribution and do not aggregate, although the average hydrodynamic diameter was increased to 129 nm due presumably to protein adsorption.

The N_2 adsorption/desorption isotherms of MSN showed a typical MCM-41 structure (type IV) with a Brunauer−Emmett−Teller (BET) surface area of 530 m^2/g and pore volume of 0.84 cm^3/g (Figure S2 in the Supporting Information). A narrow pore size distribution of 2.3 nm was obtained for mesopores using the Barrett−Joiner−Halenda (BJH) method. After Fe_3O_4 nanocrystal immobilization, the surface area and pore volume decreased to 250 m^2/g and 0.49 cm^3/g, respectively, due mainly to a significant increase in total weight of the nanocrystals (Figure 1e). Considering only the weight of silica in Fe_3O_4-MSN (based on the weight ratio of Fe_3O_4:MSN = 31:9), the

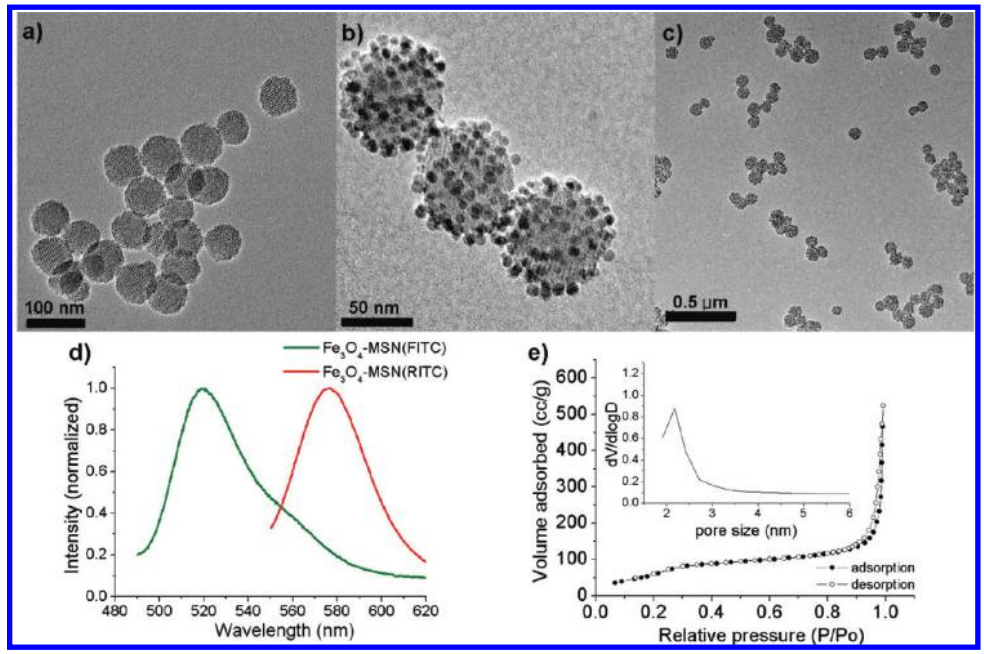

Figure 1. Characterization of synthesized Fe_3O_4-MSN. (a−c) TEM images of (a) As synthesized MSN, (b,c) Fe_3O_4-MSN. (d) Photoluminescence spectra of dye-doped Fe_3O_4-MSN. (e) N_2 adsorption/desorption isotherms of Fe_3O_4-MSN (inset: pore size distribution from adsorption branch).

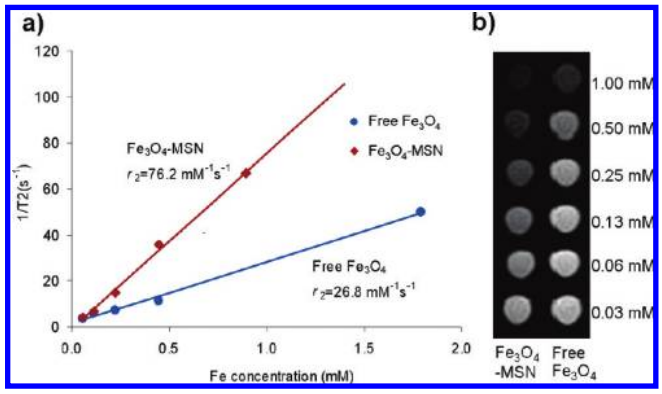

Figure 2. MR signal enhancement by Fe_3O_4-MSN. (a) Plot of inverse transverse relaxation times (1/T2) versus Fe concentration. The slope indicates the specific relaxivity value, r_2. (b) T2 weighted MR image of Fe_3O_4-MSN and free Fe_3O_4. Darker signal was observed for Fe_3O_4-MSN at the same concentration of Fe, and specific relaxivity value r_2 increased by 2.8 times as compared to free Fe_3O_4.

surface area was calculated to be 323 m^2/g. Although pores seemed to be partially blocked by Fe_3O_4 nanocrystals, the surface area of Fe_3O_4-MSN was sufficiently large for use as a drug delivery vehicle.

Because the superparamagnetic characteristics of the Fe_3O_4 nanocrystals accelerate the transverse relaxation of water protons, Fe_3O_4-MSN could be used as a T2 contrast agent in MRI. It is well reported that assembled or aggregated superparamagnetic nanoparticles can remarkably enhance MR signals due to synergistic magnetism.[11] Transverse (T2) relaxation times of protons from the dispersion containing Fe_3O_4-MSN were measured and compared to that of free Fe_3O_4 nanocrystals. The specific relaxivity value (r_2) of free Fe_3O_4 nanocrystals was 26.8 $mM^{-1}\ s^{-1}$ at 1.5 T. In contrast, Fe_3O_4-MSN showed a noticeably darker MR contrast with an increased specific relaxivity value of 76.2 $mM^{-1}\ s^{-1}$ (Figure 2). Assembly of multiple Fe_3O_4 nanocrystals on MSN indeed resulted in a remarkably enhanced MR contrast.

The cytotoxicity of Fe_3O_4-MSN was evaluated by MTT assay and trypan blue exclusion assay (Figure S3 in the Supporting Information). MTT assay revealed that cell viability was not hindered following culture with a concentration of 100 μg Fe mL^{-1} for 24 h. Trypan blue exclusion assays also showed that proliferation was not reduced in the presence of Fe_3O_4-MSN even after 72 h.

In Vitro Imaging and Drug Delivery. Cellular uptake of Fe_3O_4-MSN was verified by confocal laser scanning microscopy (CLSM) following the incubation of cells with the nanoparticles in serum containing cell culture media for 24 h. Orange fluorescence of RITC-doped MSN was observed in cytoplasm. Cellular uptake was also confirmed by Prussian blue staining (Figure S4 in the Supporting Information). The results showed that increasing the concentration of Fe_3O_4-MSN in the cell incubation media enhanced the uptake of Fe_3O_4-MSN. In both CLSM and Prussian blue staining images, the internalized Fe_3O_4-MSN were observed in the cytoplasm but not in the nucleus. The internalization of Fe_3O_4-MSN was also directly confirmed by TEM (Figure S5 in the Supporting Information).

To demonstrate in vitro multimodal imaging, fluorescence and T2 weighted MR images of the Fe_3O_4-MSN labeled cell phantom were acquired (Figure 3a,b). As the concentration of Fe_3O_4-MSN was increased during the incubation, the RITC fluorescence signal was clearly enhanced and the T2 weighted

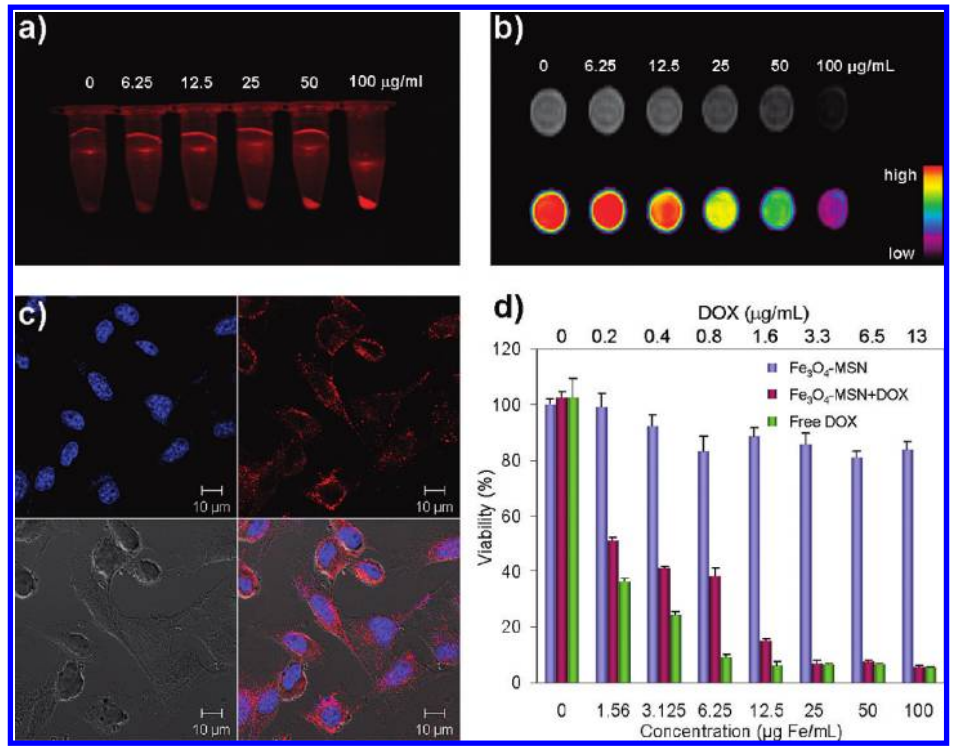

Figure 3. In vitro multimodal imaging and drug delivery with Fe_3O_4-MSN. (a) Fluorescence image of cell pellets and (b) MR (upper) and its color mapped (lower) images of dispersed cells in agarose. 1×10^6 cells were incubated with various concentrations of Fe_3O_4-MSN for 24 h. (c) Confocal laser scanning microscopic images of B16−F10 cells incubated with Fe_3O_4-MSN for 24 h. Upper left: The nuclei stained with blue 4′-6-diamidino-2-phenylindole (DAPI). Upper right: The spot-like red fluorescence showing internalized Fe_3O_4-MSN. Lower left: Differential interference contrast (DIC) image. Lower right: Merged image of blue (DAPI), red (RITC of Fe_3O_4-MSN), and DIC. (d) In vitro cytotoxicity of Fe_3O_4-MSN, DOX loaded Fe_3O_4-MSN, and free DOX against B16−F10 cell after 24 h incubation.

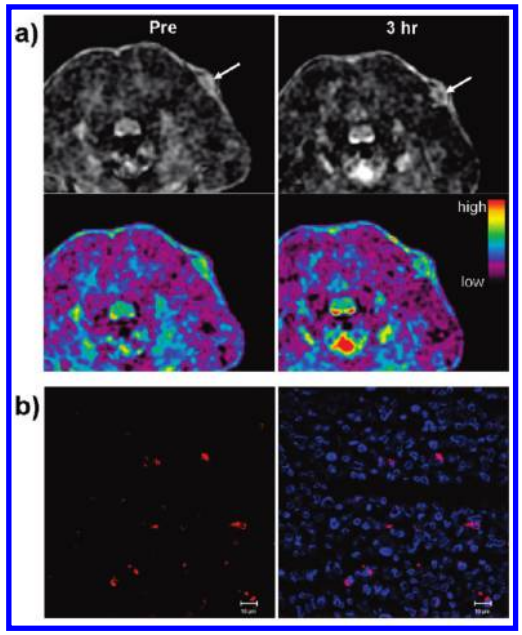

Figure 4. In vivo accumulation of Fe_3O_4-MSN at tumor site. (a) In vivo T2 weighted MR images (upper) and color mapped (lower) images of tumor site before and 3 h after intravenous injection of Fe_3O_4-MSN (arrows indicate tumor site). (b) Confocal laser scanning microscopic images of sectioned tumor tissue harvested 24 h after injection. Left: Red fluorescence showing Fe_3O_4-MSN internalized cells. Right: Merged image with DAPI stained nuclei (blue) (scale bar = 10 μm).

MR image was darkened. This demonstrates that Fe_3O_4-MSN can be used as a probe for simultaneous T2 MRI and optical fluorescence imaging. The spot-like fluorescence demonstrates that Fe_3O_4-MSN was internalized via endocytosis and remained in endosomes (Figure 3c).

To examine drug delivery, the chemotherapeutic agent doxorubicin (DOX) was loaded into Fe_3O_4-MSN. The measurement using UV−vis absorption spectroscopy revealed that approximately 0.08 mg of DOX was loaded in 1 mg of Fe_3O_4-MSN. Antitumor efficacy of DOX loaded Fe_3O_4-MSN was tested using the B16−F10 melanoma cell line (Figure 3d). The DOX-loaded Fe_3O_4-MSN and free DOX showed comparable cytotoxicities at the same concentration of DOX. This suggests that Fe_3O_4-MSN is very efficient as a drug delivery vehicle.

Passive Targeting of Fe_3O_4-MSN to Tumor Site. For exploratory in vivo animal optical and MR imaging, we subcutaneously injected MCF-7 cells labeled with Fe_3O_4-MSN and unlabeled MCF-7 cells as control into each dorsal shoulder of a nude mouse. With RITC-doped Fe_3O_4-MSN, the labeled MCF-7 cells were clearly detected as a strong red volume in the fluorescence image and as a dark volume of subcutaneous tumor in the T2 weighted MR image, while the unlabeled MCF-7 cells did not show any fluorescence signal and MR contrast enhancement in both images (Figure S7 in the Supporting Information).

It is well-known that nanoparticles can accumulate at tumors via the enhanced permeation and retention (EPR) effect, which results from extravasation into leaky vascular endothelial cells around tumors.[17] Passive targeting and accumulation of Fe_3O_4-MSN at the tumor site could be demonstrated by in vivo MR imaging. Fe_3O_4-MSN was injected intravenously into a nude mouse bearing a tumor on its shoulder.

T2 weighted MR images at 1.5 T were obtained before and after the injection. At 3 h after injection, a drop in the MR signal was detected at the tumor site, demonstrating passive targeting of Fe_3O_4-MSN caused by the EPR effect (Figure 4a). To confirm accumulation of Fe_3O_4-MSN, the mouse was sacrificed 24 h after the injection, and its tumor tissue was sectioned and observed by CLSM. The accumulation of Fe_3O_4-MSN at the tumor site was verified by orange RITC fluorescence (Figure 4b). The MR and CLSM images showed that the Fe_3O_4-MSN also accumulated in the liver, spleen, and lung via phagocytosis of macrophages (Figures S8, S9 in the Supporting Information).[18]

Delivery of drug to tumor site was demonstrated with Fe_3O_4-MSN synthesized without fluorescent dye. Nude mice bearing a tumor were given intravenous injections of free Fe_3O_4-MSN and DOX loaded Fe_3O_4-MSN. For DOX loaded Fe_3O_4-MSN, injection doses of DOX were 2 and 4 mg/kg. The mice were sacrificed 48 h after the injection, and their tumor tissues were sectioned and observed by CLSM. Red fluorescence of DOX allowed direct visualization of drug accumulation at the tumor site of mice treated with DOX loaded Fe_3O_4-MSN, while red fluorescence was hardly detected at tumor site of mouse treated with free Fe_3O_4-MSN (Figure S10 in the Supporting Information). To examine antitumor activity of the drug, apoptotic and nonapoptotic cells in tumor tissues were evaluated using terminal deoxynucleotidyl transferase-mediated nick end labeling (TUNEL) assay (Figure 5). TUNEL-positive tumor cell nuclei (brown color) with apoptotic morphology were detected in tumor tissues of mice treated with DOX loaded Fe_3O_4-MSN (Figure 5b,c), whereas apoptotic cells were rarely detectable in the case of free Fe_3O_4-MSN (Figure 5a). These results show that DOX was delivered to the tumor site successfully and its antitumor activity was retained.

Conclusions

In summary, we synthesized multifunctional nanoparticles by assembling Fe_3O_4 nanocrystals on uniform dye-doped mesoporous silica nanoparticles. The PEG-stabilized nanoparticles were

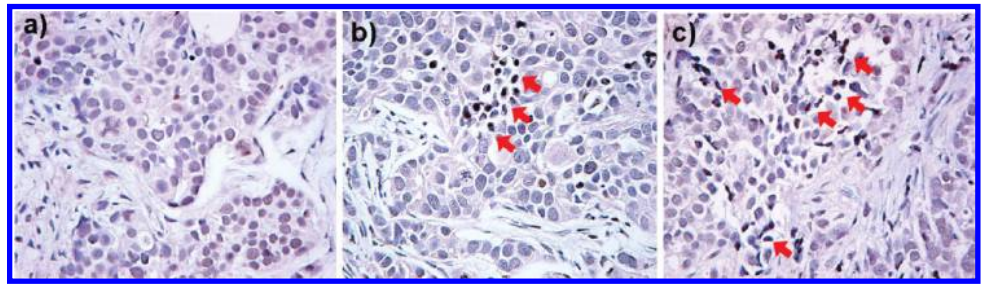

Figure 5. Terminal deoxynucleotidyl transferase-mediated nick end labeling (TUNEL) assays for apoptotic cell death. Tumor section from mouse that was given intravenous injection of (a) free Fe_3O_4-MSN as control, (b) DOX loaded Fe_3O_4-MSN (DOX 2 mg/kg), and (c) DOX loaded Fe_3O_4-MSN (DOX 4 mg/kg). Arrows indicate examples of TUNEL-positive (brown color) cells with apoptotic morphology. The mice were sacrificed 48 h after the injection.

very stable in aqueous solution and did not affect cell viability or proliferation. MR contrast was significantly enhanced following the integration of multiple superparamagnetic Fe_3O_4 nanocrystals on MSN. The composite nanoparticles were extremely versatile and have great potential as probes in MRI and fluorescence imaging as well as drug delivery carriers due to their superparamagnetic, fluorescent, and porous character. When injected through the tail vein, the composite nanoparticles accumulated at the tumor site. Through similar assembly methods, it is expected that various other kinds of nanoparticles can be immobilized on mesoporous silica nanoparticles,[15] providing versatile multifunctional nanoplatforms for biomedical applications.

Acknowledgment. T.H. thanks the Korean Ministry of Education, Science, and Technology for financial support through the National Creative Research Initiative (R16-2002-003-01001-0) and the World Class University (R31-10013) Programs of the National Research Foundation of Korea (NRF). W.K.M. thanks the financial support from the Innovative Research Institute for Cell Therapy, Korea (A062260).

Supporting Information Available: Detailed experimental procedures, hydrodynamic size distribution of Fe_3O_4-MSN by dynamic light scattering (DLS), N_2 adsorption/desorption isotherms of MSN, in vitro cytotoxicity test of Fe_3O_4-MSN, Prussian blue staining and TEM images of cell after incubation with Fe_3O_4-MSN, release profile of DOX, in vivo multimodal imaging, T2 weighted MR images of mouse and CLSM images of sectioned tissues from various organs after intravenous administration of Fe_3O_4-MSN, and CLSM images of sectioned tumor tissues after intravenous administration of DOX loaded Fe_3O_4-MSN. This material is available free of charge via the Internet at http://pubs.acs.org.

JA905793Q

(15) Kim, J.; Lee, J. E.; Lee, J.; Jang, Y.; Kim, S.-W.; An, K.; Yu, J. H.; Hyeon, T. *Angew. Chem., Int. Ed.* **2006**, *45*, 4789.
(16) Harris, J. M.; Chess, R. B. *Nat. Rev. Drug Discovery* **2003**, *2*, 214.
(17) (a) Peer, D.; Karp, J. M.; Hong, S.; Farokhzad, O. C.; Margalit, R.; Langer, R. *Nat. Nanotechnol.* **2007**, *2*, 751. (b) Brigger, I.; Dubernet, C.; Couvreur, P. *Adv. Drug Delivery Rev.* **2002**, *54*, 631.
(18) (a) Josephson, L.; Kircher, M. F.; Mahmood, U.; Tang, Y.; Weissleder, R. *Bioconjugate Chem.* **2002**, *13*, 554. (b) Sun, X.; Rossin, R.; Turner, J. L.; Becker, M. L.; Joralemon, M. J.; Welch, M. J.; Wooley, K. L. *Biomacromolecules* **2005**, *6*, 2541.